Order to disorder transition due to entropy in layered and 2D carbides

Brian C. Wyatt [1], Yinan Yang [2], Paweł Michałowski [3*], Tetiana Parker [4], Yamilée Morency [5], Francesca Urban [4], Givi Kadagishvili [6], Manushree Tanwar [6], Sixbert P. Muhoza [7], Srinivasa Kartik Nemani [8], Annabelle Bedford [1], Hui Fang [6], Zachary D. Hood [7], Junwoo Jang [8], Krutarth Kamath [1], Bethany G. Wright [8], Rebecca Disko [8], Anupma Thakur [1], Sanguk San [5], Neil Ghosh [8], Xianfan Xu [8], Zahra Fakhraai [6*], Yury Gogotsi [4*], Aleksandra Vojvodic [5*], De-en Jiang [2*], Babak Anasori [1,8*]

[1] School of Materials Engineering, Purdue University, West Lafayette, IN 47907, USA
[2] Department of Chemical and Biomolecular Engineering, Vanderbilt University, Nashville, TN 37235, USA
[3] Łukasiewicz Research Network - Institute of Microelectronics and Photonics, Warsaw, Poland
[4] A.J. Drexel Nanomaterials Institute and Department of Material Science and Engineering, Drexel University, Philadelphia, PA 19104, USA
[5] Department of Chemical and Biomolecular Engineering, University of Pennsylvania, Philadelphia, Pennsylvania 19104, USA
[6] Department of Chemistry, University of Pennsylvania, Philadelphia, PA 19104, USA
[7] Applied Materials Division, Argonne National Laboratory, Lemont, IL 60439, USA
[8] School of Mechanical Engineering, Purdue University, West Lafayette IN 47907, USA

*Corresponding authors. Email: banasori@purdue.edu, de-en.jiang@vanderbilt.edu, alevoj@seas.upenn.edu, gogotsi@drexel.edu, fakhraai@sas.upenn.edu, pawel.michalowski@imif.lukasiewicz.gov.pl

Abstract:

There is controversy surrounding the moniker "high-entropy" materials due to the unclear effect of entropy and enthalpy. The unique nanolayered structure of MAX phases, with its structural covalent-metallic-covalent carbide interfaces, allowed us to address this controversy systematically. Here, we synthesized nearly 40 known and novel MAX phases containing 2 to 9 metals and found that their enthalpic preference for short-range order remains until entropy increases enough to achieve all configurations of the transition metals in their atomic planes. In addition, we transformed all these MAX phases into two-dimensional (2D) MXenes and showed the effects of the order vs. disorder on their surface properties and electronic behavior. This study indicates that short-range ordering in high-entropy materials determines the impact of entropy vs. enthalpy on their structures and properties.

Main text:

Alloys containing stoichiometric mixtures of metallic elements in high-entropy alloys were systematically explored in the early 2000s (*1, 2*), and demonstrated increased mechanical properties (*3*) and decreased thermal conductivity (*4*) beyond normal expectations of the "rule of mixture" approximations (*3-7*). In one of the early studies (*1*), it was proposed that increasing the number of these metals could result in entropy-stabilization of enthalpically unfavorable mixtures of elements. This has been shown in metallic alloys (*8*), carbides (*9*), oxides (*10*), diborides (*11*), and other ceramics (*12*).

Early on, such entropy-stabilized structures took on the moniker of "high-entropy", which was due to the large contribution of entropy in Gibbs' free energy. However, since this moniker became popular, there has been pushback to using "high-entropy" as a general label (*13*), as it can obfuscate the major effect enthalpy still has on the stability of a single-phase system. For example, short-range ordering in some high-entropy systems (*14-17*) suggests that enthalpic effects must still be present. Thus, while configurational entropy can stabilize some single-phase structures that are enthalpically resistant to form, it alone may not be enough to stabilize *all* possible configurations (*18*). Therefore, there is a fundamental need to evaluate the true role of entropy vs. enthalpy in the achieved configurations in single-phase "high-entropy" materials. This study aims at the understanding of the entropy role in overcoming short-range ordering in MAX phases, a large family of layered transition metal carbides and nitrides. Their layered structure with 2 to 5 atomic layers of transition metals and ability to form solid solutions provide a unique platform for addressing the above fundamental question.

MAX phases are chemically denoted by their formula $M_{n+1}AX_n$, where M refers to n+1 layers of one or more early transition metals that are interleaved by X, which represents n layers of carbon/nitrogen (*19*). Between these $M_{n+1}X_n$ slabs, there are monoatomic layers of one or more A elements (*20*). M is ionic/covalently bound to X (*21*), similar to a transition metal carbide (*22*), while the surface M of each $M_{n+1}X_n$ slab is metallically bound to the A element (*21*), which is structurally similar to a stacking fault in layered ceramics (*23, 24*). As a result of this different structure and bonding at the $M_{n+1}X_n$-A-$M_{n+1}X_n$ interface, there can be a preference for ordering of two or more transition metals in separate transition metal planes (*25*). When n is more than 1 in $M_{n+1}AX_n$, some transition metals prefer M sites bound to both X and to A (M' layers) or M sites only bound to X (M″), which is referred to as o-MAX (Figure 1a for M = 2) (*26-28*).

Although these o-MAX phases were reported a decade ago (*29*), the preference for an M′ vs. an M″ site in MAX phases is not fully understood. Computationally, it has been shown that Group 6 transition metals, such as Cr, Mo, and W prefer M' sites while Group 4 transition metals, such as Ti, Zr, and Hf prefer M″ sites (*30, 31*). Similarly, the earliest reported "high-entropy" MXenes, in 2021, $(TiVCrMo)_4C_3$ and $(TiVNbMo)_4C_3$ (*32*), still predicted to prefer Cr and Mo in M' sites and Ti and Nb in M″ sites (*33*). As MXenes are derived from their precursor MAX phases (*34*), this suggests that even in entropy-stabilized MAX phases (*32*), this enthalpic preference of M' or M″ site occupancy is likely present. To the point of this work, MAX and MXenes provide a unique material system to evaluate the short-range ordering in multi-elemental materials and demonstrate the effects of enthalpy vs. entropy on the order-to-disorder transition at the smallest scale (i.e., a few layers of atoms). This work establishes the synthesis of multi-transition metal MAX phases, the trends in the ordering and disordering of their M layers due to enthalpy and entropy, and demonstrates some of the surface and electronic properties of their synthesized MXenes.

Effect of enthalpy and entropy on the order-to-disorder transition in MAX phases

To gain insight into the competition between enthalpy and entropy toward the order-disorder transition in high-entropy MAX phases (Figure 1a), we first used density functional theory (DFT). To understand the M′ vs. M″ preference for different transition metals in the M_4AlC_3 MAX phase, we built a symmetric model considering a pair (M_1 and M_2) of transition metals in either M′ or M″ layers (M_1-M_2-M_2-M_1) for all the possible combinations (from 2 to 9 elements) (Figure S1). Figure S2 shows the formation energy (E_f) above the hull energy of these configurations; the calculation details are reported in the supporting information.

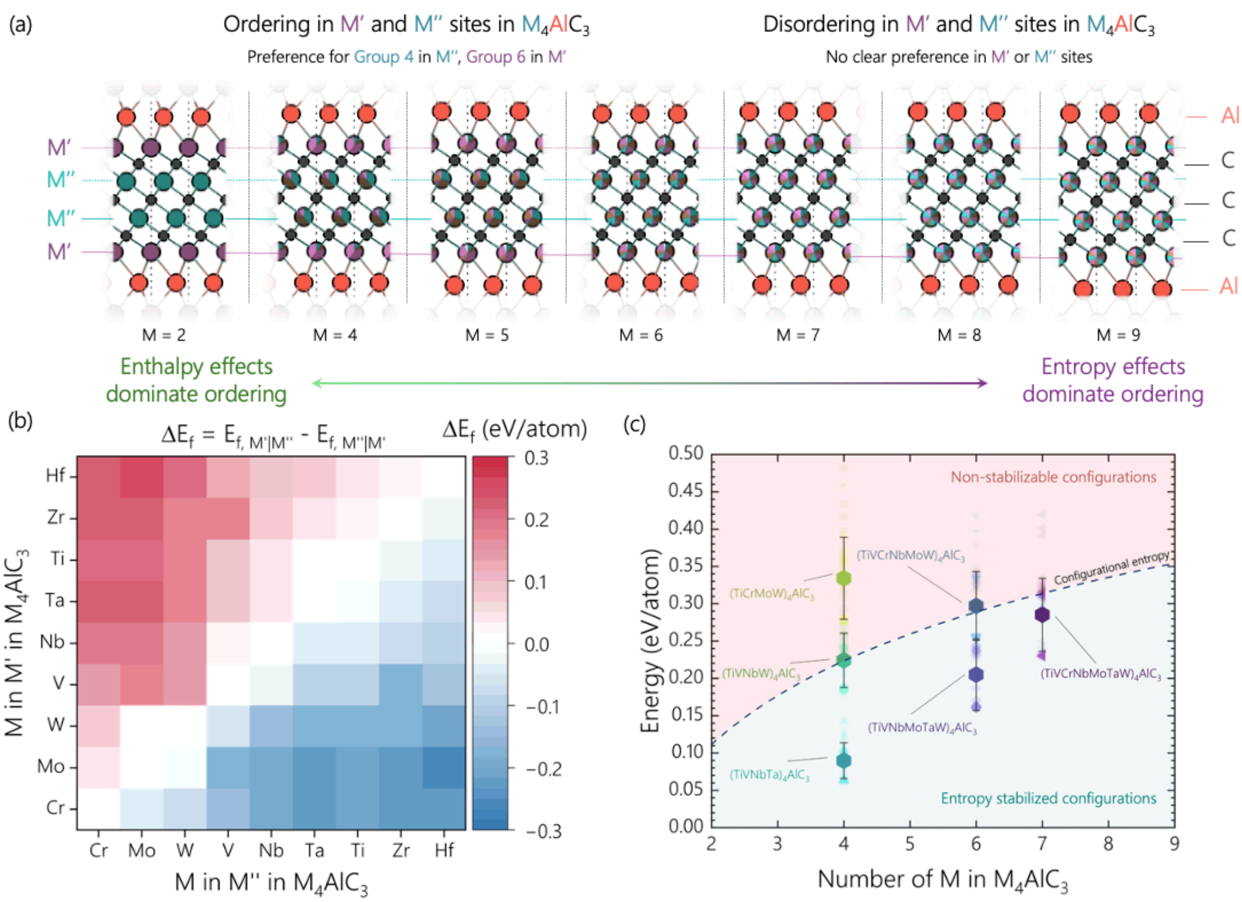

Fig. 1. Enthalpy vs. entropy competition toward order-disorder in M_4AlC_3 MAX phases. (A) Schematic showing the hypothesis of increasing disorder with increasing entropy in M_4AlC_3 MAX phases. **(B)** The difference in formation

energies for different pairs of transition metals in either M′ or M′′ sites in M_4AlC_3 MAX. **(C)** Formation energy above the hull energy (energy barrier) vs. entropy in M_4AlC_3 MAX phases with the formation energy vs. entropy-crossover around 7 transition metals.

After calculating these formation energies, we next used the difference in the formation energy (ΔE_f) between these structures with two given transition metals in either M′ and M″ sites to observe the enthalpic preference of the transition metals to the various lattice sites (Figure 1b). We focused on identifying the preference for an M to order in separate transition metal planes as we found it has a higher effect on the formation energy than any in-plane order (Figure S4-5). Trend-wise, we observed that the M′ preference is Cr > Mo > W > V > Nb > Ta > Ti > Zr > Hf (inverse for M″ preference), which agrees with previous works (*30*). This preference is still present in M_4AlC_3 structures with >2 transition metals (Figure S3).

We used our model for short-range order to evaluate this argument, given the clear preference for transition metal arrangement in the M_4AlC_3 MAX phase structure. As shown in Figure 1e, we first analyzed the M_4AlC_3 MAX phase structures with 4 transition metals: $(TiVNbTa)_4AlC_3$, $(TiVNbW)_4AlC_3$, and $(TiCrMoW)_4AlC_3$. Broadly, we find when the preference for order (labeled “ordered”) is matched (Figure S4-6), the lowest formation energies are achieved. For example, when V and W occupy only M′ (outer) sites and Ti and Nb occupy only M″ (inner) sites in $(TiVNbW)_4AlC_3$, the formation energy is -0.544 ± 0.001 eV/atom. In contrast, if Ti and Nb occupy only M′ sites and V and W occupy only M″ sites (labeled “inverse ordered”), the formation energy is -0.430 ± 0.001 eV/atom. Similarly, solid solution occupancies of Ti and Nb in M′ and M″ sites have a higher formation energy of -0.485 ± 0.006 eV/atom for $(TiVNbW)_4AlC_3$ than the ordered configuration.

Additionally, we found that group 6 elements increased the distribution of the energy barriers as group 6 elements prefer M′ over M″ sites (Figure S6). This suggests that MAX phases containing mixtures without group 6 elements are more energetically favored. However, we found that the formation energy of MAX phases containing group 6 elements decreased with the increasing number of transition metals, potentially providing an avenue to include more group 6 elements in the single lattice. From another perspective, if we aim to retain group 6 elements within the system for better hydrogen evolution reaction performance, introducing increasing amounts of other transition metal (TM) elements can also enhance the system's stability and the barrier between ordering and disordering structures (Figure S6-c), thereby facilitating the transition from an ordered to a disordered structure. Due to the extensive computational demand, it is not feasible to simulate all possible compositions. Therefore, based on analyzing the contributions of enthalpy and entropy across several compositions, we predict that the transition from order to disorder likely occurs when a seventh element is introduced (Figure 1c).

With the gained knowledge from the energetic perspective, we next experimentally synthesized M_4AlC_3 MAX phases containing combinations of 2 and 4 to 9 elements of Group 4, 5, and 6 transition metals (Figure 2a-b). Synthesis and other details for the MAX phases are in the supporting information. To see if we experimentally observed ordering in our M_4AlC_3 MAX phases, we first analyzed the x-ray diffraction (XRD) patterns (Figure S7-8). All of the reported phases in this work can be found in Table S1. All MAX phase characterization and analysis for each phase reported can be found in Figures S9-34. Figure 2c shows the scanning electron microscopy (SEM) image of $(TiVCrZrNbMoHfTaW)_4AlC_3$ with a layered grain structure; the energy dispersive X-ray spectroscopy (EDS) shows that the grain contains all 9 transition metals as well as Al (Figure 2d). Although the XRD data gave us some insight into the ordering, it is difficult to accurately compare transition metals with very similar X-ray scattering behaviors (i.e., Ti vs. V or Cr, Zr vs. Nb or Mo, Hf vs. Ta or W), so we focused on using an atomic-layer resolved dynamic secondary ion mass spectrometry (SIMS) method (*35-37*).

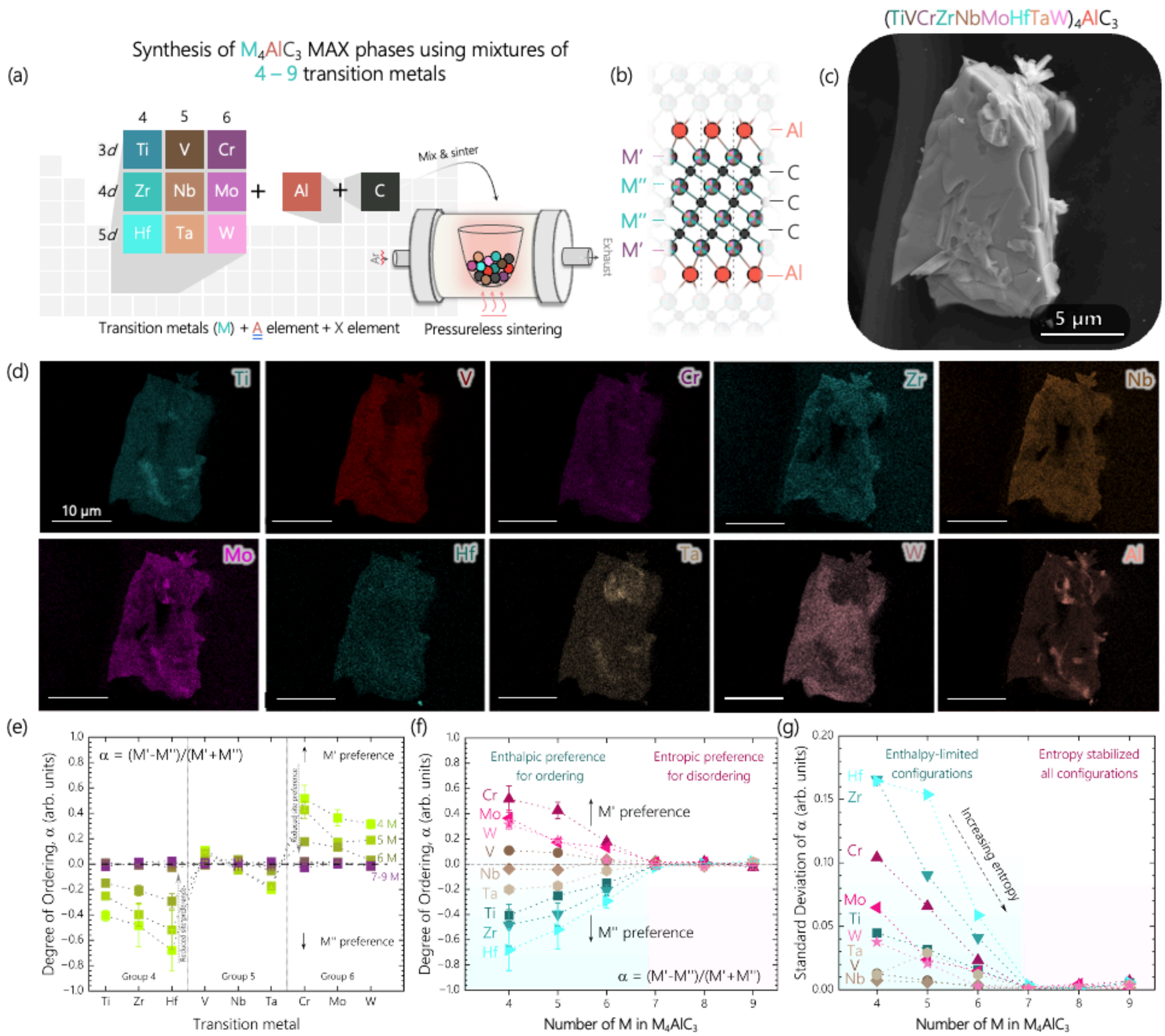

Fig. 2. Synthesis and analysis of $(TiVCrZrNbMoHfTaW)_4AlC_3$ and other M_4AlC_3 phases containing 2 to 9 transition metals. (A) Schematic highlighting the mixed elements and synthesis approach. **(B)** Crystal structure of the targeted M_4AlC_3 MAX phase. **(C)** Electron microscopy image of a grain of $(TiVCrZrNbMoHfTaW)_4AlC_3$ MAX. **(D)** Elemental mapping of a grain of $(TiVCrZrNbMoHfTaW)_4AlC_3$ MAX showing the presence of all 9 transition metals and aluminum. **(E)** Secondary ion mass spectrometry (SIMS) measurements show the preference for sites based on the transition metal and the total number of transition metals in M_4AlC_3 MAX. **(F)** SIMS shows the decreasing preference for

https://doi.org/10.26434/chemrxiv-2025-7f2c4 ORCID: https://orcid.org/0000-0002-1955-253X Content not peer-reviewed by ChemRxiv.

different sites in M_4AlC_3 MAX plotted against the increasing numbers of transition metals. **(G)** Decrease in standard deviation in the ordering term a as calculated by SIMS plotted against the increasing numbers of transition metals.

SIMS indicates that Mo always occupies the M′ site and Ti, V, and Nb always occupy the M″ site for equimolar M mixtures in the M_4AlC_3 MAX phases (Figure S35). This agrees with Figure 1c, which states that Group 6 transition metals primarily occupy M′ sites while Group 4 or 5 occupy M″ sites. Further, to calculate this site preference for our M_4AlC_3 MAX phases with 4 or more transition metals, the difference in the atomic composition of each element in the M′ and M″ sites was divided by their sum to create an "α" parameter, where a positive α indicates a given M prefers the M′ site and a negative α indicates that a given M prefers the M″ site, respectively. Using this parameter, we noted that when 4 transition metals were placed into the M_4AlC_3 MAX phase, the trend in preference of a transition metal for an M′ or M″ site was the same as established for M_4AlC_3 MAX with two transition metals (Cr > Mo > W > V > Nb > Ta > Ti > Zr > Hf in M′ site) (Figure 2e). This agrees with Figure 1c, suggesting that an enthalpic preference for M′ or M″ site ordering of the transition metals is still present even for these entropy-stabilized M_4AlC_3 MAX phases (*32*).

Further, we observed that increasing the number of transition metals to 5 and 6 resulted in a diminished $|\alpha|$ for each transition metal (Figure 2f). Together with Figure 1c, this suggests that configurations with less preference for order are more likely to be stabilized by the increasing configurational entropy. For the SIMS data, this would result in a lower $|\alpha|$ for each transition metal, as ordered (following Figure 1b), *and* disordered configurations of the transition metals would become observable in each transition metal layer. Probabilistically, however, we would not expect $|\alpha|$ to converge on zero yet in these low-to-medium entropy systems, as inverse-ordered configurations would not yet become stabilizable through entropy.

Conversely, beyond 7 transition metals, we observe that the $|\alpha|$ converges on 0 for all transition metals (Figure 2f). The convergence of $|\alpha|$ to zero suggests that ordered, solid solution, and inverse ordered configurations are stabilized. This would likely result in equal probabilistic chances to observe any configuration via SIMS measurements. We see further support for this hypothesis by plotting the standard deviation of $|\alpha|$ for all transition metals against the total number of transition metals (Figure 2f), which further suggests that all configurations become stabilized at ≥7 transition metals. Overall, our computational and experimental results indicate that the loss of short-range ordering in high-entropy MAX phases is only achievable once entropy can overcome the enthalpic barriers for all configurations. Broadly, this data demonstrates that (i) entropy-stabilized systems *can* display a preference for short-range ordering, but (ii) systems only truly become "high-entropy" materials once entropy overcomes any remaining enthalpic preferences for the short-range order.

Effect of order vs. disorder on MXenes

After confirming the synthesis and ordering behavior of the M_4C_3 structure in the M_4AlC_3 MAX phases, we evaluated the effect of order vs. disorder and composition on the individual M_4C_3 lamellas. To do so, we synthesized the $M_4C_3T_x$ MXenes from their M_4AlC_3 MAX phases using wet chemical synthesis (Figure 3a) (*28, 31, 32, 34*), which causes the MXene surface to be terminated with T_x groups, commonly -O, -(OH), and -F (*34*). 2D flakes of MXenes are shown in Figures S36-38. Further, we confirmed that our MXenes contained the same transition metals as the MAX, as shown for $(TiVCrZrNbMoHfTaW)_4C_3T_x$ in Figures S37-38. Although all 2D MXenes produced in this study were stable in water (Figure S39), using X-ray photoelectron spectroscopy (XPS), we observed that the overall composition of T_x in the $M_4C_3T_x$ MXenes containing 4 to 9 transition metals increased for -O (~33 at% to ~53 at%) and decreased for -OH (~37 at% to ~26 at%) and -F (~30 at% to 21 at%) (Figure S40-48 & Table S2).

The ordering/disordering observed in the MAX phases would be present in the MXenes (*36*) and could be the source of the changes in the T_x group composition in the respective $M_4C_3T_x$ MXenes. To gain insight into this trend, we used DFT to calculate the formation energy of -O and -F terminations on MXenes with different pairs of transition metals in either M′ or M″ sites (Figure 3b). We observed that pairs of Group 4 elements prefer F terminations, and pairs of Group 6 elements prefer O terminations. We also observed that Group 6 in M″ causes an increased preference for Group 4 in M′ for O terminations, and Group 4 in M″ causes an increased preference for Group 6 in M′ for F terminations. As shown in the supporting information (Figure S49), the solid solution combinations are typically between the two ordered configurations. The calculated values of O vs. F preference for both ordered and solid solution configurations of the paired transition metals are shown in Figure S50.

As we cannot know the subsurface M″ metal for any given M′ metal bound to T_x in our MXenes, we chose to plot the surface chemistry for Ti and W in M′ sites (bound to T_x) against the valence electron concentration (VEC) in the M″ sites, which was derived from SIMS using formal charges of the transition metals (Ti has 4 VE, V has 5 VE, Cr has 6 VE, *etc*.). In addition, in this plot, we consider both –(OH) and –F terminations together and –O terminations separate, as –(OH) and –F would prefer a T^{-} oxidation state while –O would prefer a T^{2-} oxidation state. We chose to add –(OH) and –F together as our use of tetramethylammonium hydroxide as a delamination agent can replace –F groups with –(OH) groups, and the two share a formal charge. Using this plot, we see that increasing the VEC in the M″ sites can increase the concentration of O terminations on Ti and –(OH)/F on V and Mo, which is broadly in agreement with the trends shown in Figure 3b. A plot for easier comparison can be found in Figure S51. We see agreement with the general increase of O as a T_x group on $M_4C_3T_x$ MXenes containing 4 to 9 transition metals (Fourier-transform infrared spectra in Figure S52). In addition, through ultra-violet-visible-near infrared (UV-vis-NIR) and Raman spectroscopy, we gained some insight into the effect of disorder in our $M_4C_3T_x$ MXenes by increasing the total number of transition metals (Figures S53-56). Overall, this suggests surface vs. subsurface transition metals impact the chemical behavior and preference for surface terminations of the MXenes (*38*). As previous works show that the basal plane of MXenes is catalytically active (*39*), future studies should focus on the catalytic applications and the effect of surface composition on catalytic activity.

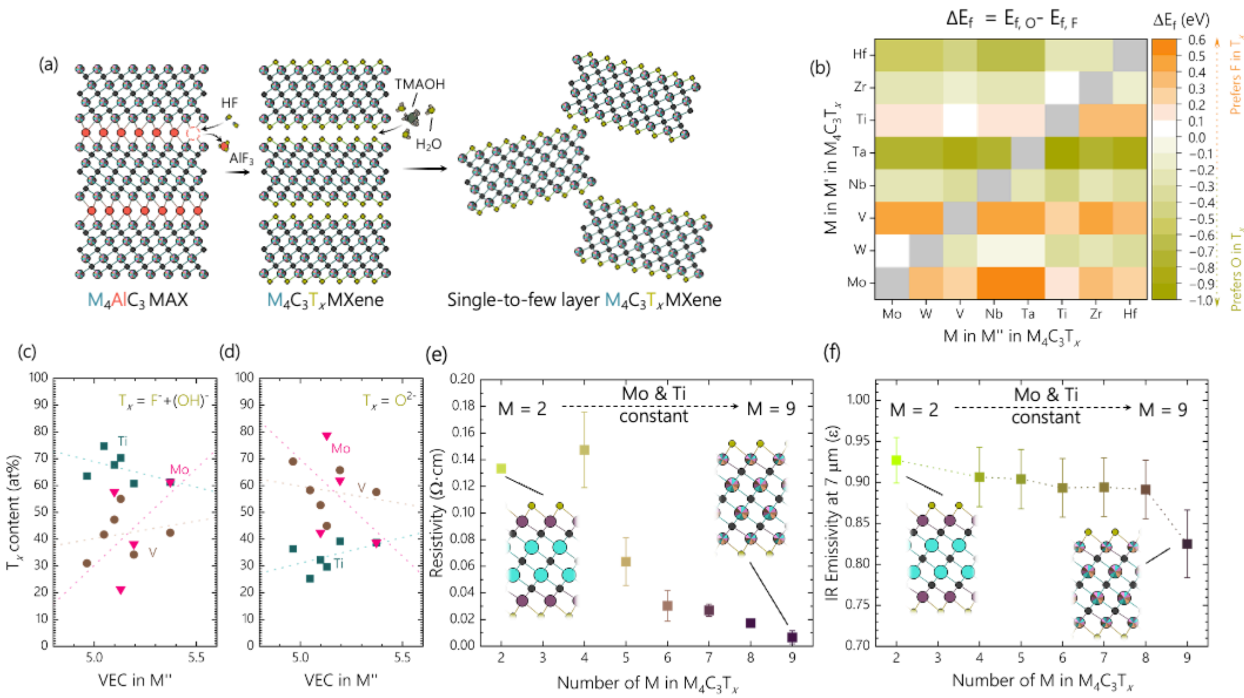

Fig. 3. Synthesis, surface chemistry, and properties of $M_4C_3T_x$ MXenes containing 2 to 9 transition metals. (A) Schematic of the synthesis process of $M_4C_3T_x$ MXenes from M_4AlC_3 MAX. **(B)** Differences in formation energy of pairs of transition metals in $M_4C_3T_x$ with O vs. F in T_x. The greyed boxes represent values that have yet to be calculated. **(C-D)** Content of O and F terminations, respectively, on Ti, V, and Mo atoms in $M_4C_3T_x$ MXenes vs. the valence electrons concentration (VEC) in the M'' layers. The dotted lines are guides for the eye. **(E)** Electrical resistivity behavior of $M_4C_3T_x$ MXenes containing 2 to 9 transition metals. **(F)** IR emissivity at 7 mm wavelength plotted against the total number of transition metals in the $M_4C_3T_x$ MXenes.

Next, we evaluated the effect of multiple transition metals and order vs. disorder on the electrical properties of thin films of these $M_4C_3T_x$ MXenes. When we investigated the $M_4C_3T_x$ MXenes containing 2 to 9 transition metals, we found that the MXenes retain their metallic conductivity by both their linear *I* vs. *V* behavior as well as their consistency with the Drude model of metallic electrical conductivity (Figure S57-63) (*40*). In addition, we noted that MXenes that contained Cr were up to an order of magnitude higher in electrical resistivity (Figure S64), which is reported for high-entropy alloys (*41*). The flake sizes are shown using dynamic light scattering measurements in Figure S65. In Figures S63-71, atomic force microscopy images, height, and surface roughness analysis of some of the $M_4C_3T_x$ flakes containing 2 – 9 transition metals are shown (Table S3 summarizes the height and surface roughness results).

In previous literature, decreasing electrical resistivity has been reported for increasing numbers of transition metals in high-entropy alloys (*42*). However, the cause is not yet fully understood. In M_2C-type MXenes, computational work has shown Group 5 transition metals in

MXenes should lower the electrical resistivity (*43*) while Group 6 transition metals MXenes have a higher electrical resistivity (*44*). Overall, in our high-entropy $M_4C_3T_x$ MXenes, we expect an increasing number of transition metals to cause disorder of Group 5 and 6 transition metals throughout the $M_4C_3T_x$ structure. Therefore, we first plotted the electrical conductivity of our $M_4C_3T_x$ MXenes against the total number of transition metals, as shown in Figure 4d. In Figure 4d, we chose to keep Ti and Mo as consistent transition metals, and systematically add one transition metal at a time to maintain comparability between samples. For example, at M = 2, we show the fully ordered $Mo_2Ti_2C_3T_x$, at M = 4 we show the low entropy $(TiVNbMo)_4C_3T_x$, and then add W, Ta, Cr, Zr, and Hf for M = 5, 6, 7, 8, and 9, respectively.

In this plot, we can see the original resistivity of $Mo_2Ti_2C_3T_x$ at 0.13 Ω·cm, which initially increases for $(TiVNbMo)_4C_3T_x$ to 0.15 ± 0.03 Ω·cm, and then decreases to 0.01 ± 0.01 Ω·cm $(TiVCrZrNbMoHfTaW)_4C_3T_x$. In addition, we observed a similar behavior of the infrared (IR) emissivity behavior of these MXenes (Figure 3f). This agrees with the changes in electrical resistivity shown in Figure 3e, as decreasing electrical resistivity typically will result in a proportional decrease in IR emissivity (*45*). Broadly, we hypothesize that this decrease in resistivity could be attributed to two reasons (Figure S75): 1) the decrease in ordering results in fewer neighbors of Group 6 to Group 6 transition metals, or 2) the decrease in order creates structures with smaller differences in the total number of valence electrons (averaging to 5) between neighbors in both M′ and M″ layers, both of which could improve the electron mobility in the M′ and M″ layers. However, future studies are necessary to better understand the electron mobility and other properties in high-entropy MXenes and other high-entropy materials (*46*), such as approaches that focus on single-flake measurements or optical conductivity (Figure S73).

In summary, this work demonstrates a broad advancement in the understanding of the relation of enthalpy and entropy on short-range ordering in high-entropy materials. Specifically, by using M_4AlC_3 MAX phases with 2 to 9 transition metals and analyzing their structural ordering using SIMS, we were able to evaluate the trend in the short-range ordering of transition metals in either outer (M′) or inner (M″) metal sites against the total number of transition metals. Doing so, we have shown that 1) in low and medium entropy combinations (up to 6 metals), the transition metals enthalpically prefer order in M′ or M″ sites, 2) at 7 metals or above, the structures become fully disordered (no clear preference for M′ or M″), and that this order-disorder transition was 3) driven by an increasing contribution of configurational entropy. Lastly, we showed that these MAX phases can be used to synthesize their respective MXenes, which allowed us to observe some effects of entropic-driven disorder in these phases on the electrical and IR emissivity properties of the derived MXenes. Within layered ceramics and 2D material research, this article represents an advancement in the synthesis of MAX and MXenes containing up to 9 transition metals, thus expanding the families of these materials. For the broad scientific community, this work represents major progress in understanding the role of enthalpy and entropy in the formation and order-disorder transitions in high-entropy materials.

References and Notes

1. J. W. Yeh *et al.*, Nanostructured high-entropy alloys with multiple principal elements: novel alloy design concepts and outcomes. *Advanced Engineering Materials* **6**, 299-303 (2004).
2. B. Cantor, I. Chang, P. Knight, A. Vincent, Microstructural development in equiatomic multicomponent alloys. *Materials Science and Engineering: A* **375**, 213-218 (2004).
3. D. Utt *et al.*, The origin of jerky dislocation motion in high-entropy alloys. *Nature Communications* **13**, 4777 (2022).
4. H.-P. Chou, Y.-S. Chang, S.-K. Chen, J.-W. Yeh, Microstructure, thermophysical and electrical properties in AlxCoCrFeNi (0≤ x≤ 2) high-entropy alloys. *Materials Science and Engineering: B* **163**, 184-189 (2009).
5. L. Han *et al.*, Multifunctional high-entropy materials. *Nature Reviews Materials* **9**, 846-865 (2024).
6. S. Schweidler *et al.*, High-entropy materials for energy and electronic applications. *Nature Reviews Materials* **9**, 266-281 (2024).
7. Y. Zhang, T. Zuo, Y. Cheng, P. K. Liaw, High-entropy alloys with high saturation magnetization, electrical resistivity and malleability. *Scientific Reports* **3**, 1455 (2013).
8. F. Otto, Y. Yang, H. Bei, E. P. George, Relative effects of enthalpy and entropy on the phase stability of equiatomic high-entropy alloys. *Acta Materialia* **61**, 2628-2638 (2013).
9. P. Sarker *et al.*, High-entropy high-hardness metal carbides discovered by entropy descriptors. *Nature Communications* **9**, 4980 (2018).
10. C. M. Rost *et al.*, Entropy-stabilized oxides. *Nature Communications* **6**, 8485 (2015).
11. J. Gild *et al.*, High-entropy metal diborides: a new class of high-entropy materials and a new type of ultrahigh temperature ceramics. *Scientific Reports* **6**, 37946 (2016).
12. C. Oses, C. Toher, S. Curtarolo, High-entropy ceramics. *Nat. Rev. Mater.* **5**, 295-309 (2020).
13. M. Brahlek *et al.*, What is in a name: Defining “high entropy” oxides. *APL Materials* **10**, (2022).
14. S. Chen *et al.*, Simultaneously enhancing the ultimate strength and ductility of high-entropy alloys via short-range ordering. *Nature Communications* **12**, 4953 (2021).
15. P. Singh, A. V. Smirnov, D. D. Johnson, Atomic short-range order and incipient long-range order in high-entropy alloys. *Physical Review B* **91**, 224204 (2015).
16. A. J. Wright, J. Luo, A step forward from high-entropy ceramics to compositionally complex ceramics: a new perspective. *Journal of Materials Science* **55**, 9812-9827 (2020).
17. B. Jiang *et al.*, Probing the local site disorder and distortion in pyrochlore high-entropy oxides. *Journal of the American Chemical Society* **143**, 4193-4204 (2020).
18. S. Divilov *et al.*, Disordered enthalpy–entropy descriptor for high-entropy ceramics discovery. *Nature* **625**, 66-73 (2024).

19. M. Dahlqvist, M. W. Barsoum, J. Rosen, MAX phases–Past, present, and future. *Materials Today* **72**, 1-24 (2024).
20. M. Sokol, V. Natu, S. Kota, M. W. Barsoum, On the Chemical Diversity of the MAX Phases. *Trends in Chemistry* **1**, 210-223 (2019).
21. M. Magnuson, M. Mattesini, Chemical bonding and electronic-structure in MAX phases as viewed by X-ray spectroscopy and density functional theory. *Thin Solid Films* **621**, 108-130 (2017).
22. B. C. Wyatt, S. K. Nemani, G. E. Hilmas, E. J. Opila, B. Anasori, Ultra-high temperature ceramics for extreme environments. *Nature Reviews Materials*, 1-17 (2023).
23. A. Gusev, A. Kurlov, V. Lipatnikov, Atomic and vacancy ordering in carbide ζ-Ta4C3− x (0.28⩽ x⩽ 0.40) and phase equilibria in the Ta–C system. *Journal of Solid State Chemistry* **180**, 3234-3246 (2007).
24. C. R. Weinberger, G. B. Thompson, Review of phase stability in the group IVB and VB transition-metal carbides. *J. Am. Ceram. Soc.* **101**, 4401-4424 (2018).
25. M. Dahlqvist, J. Rosen, The rise of MAX phase alloys–large-scale theoretical screening for the prediction of chemical order and disorder. *Nanoscale* **14**, 10958-10971 (2022).
26. W. Hong, B. C. Wyatt, S. K. Nemani, B. Anasori, Double transition-metal MXenes: Atomistic design of two-dimensional carbides and nitrides. *MRS Bulletin* **45**, 850-861 (2020).
27. B. Anasori *et al.*, Experimental and theoretical characterization of ordered MAX phases Mo_2TiAlC_2 and $Mo_2Ti_2AlC_3$. *Journal of Applied Physics* **118**, (2015).
28. B. C. Wyatt *et al.*, Design of Atomic Ordering in $Mo_2Nb_2C_3T_x$ MXenes for Hydrogen Evolution Electrocatalysis. *Nano Letters*, (2023).
29. Z. Liu *et al.*, (Cr 2/3 Ti 1/3) 3 AlC 2 and (Cr 5/8 Ti 3/8) 4 AlC 3: New MAX-phase Compounds in Ti–Cr–Al–C System. *Journal of the American Ceramic Society* **97**, 67-69 (2014).
30. M. Dahlqvist, J. Rosen, Predictive theoretical screening of phase stability for chemical order and disorder in quaternary 312 and 413 MAX phases. *Nanoscale* **12**, 785-794 (2020).
31. B. Anasori *et al.*, Two-Dimensional, Ordered, Double Transition Metals Carbides (MXenes). *ACS Nano* **9**, 9507-9516 (2015).
32. S. K. Nemani *et al.*, High-Entropy 2D Carbide MXenes: $TiVNbMoC_3$ and $TiVCrMoC_3$. *ACS Nano* **15**, 12815-12825 (2021).
33. Z. Leong *et al.*, Elucidating the Chemical Order and Disorder in High-Entropy MXenes: A High-Throughput Survey of the Atomic Configurations in TiVNbMoC3 and TiVCrMoC3. *Chem. Mater.* **34**, 9062-9071 (2022).
34. K. R. G. Lim *et al.*, Fundamentals of MXene synthesis. *Nature Synthesis* **1**, 601–614 (2022).
35. P. P. Michałowski *et al.*, Oxycarbide MXenes and MAX phases identification using monoatomic layer-by-layer analysis with ultralow-energy secondary-ion mass spectrometry. *Nature Nanotechnology* **17**, 1192-1197 (2022).

36. B. C. Wyatt *et al.*, Alkali cation stabilization of defects in 2D MXenes at ambient and elevated temperatures. *Nature Communications* **15**, 6353 (2024).
37. P. P. Michałowski, Unraveling the composition of each atomic layer in the MXene/MAX phase structure–identification of oxycarbide, oxynitride, and oxycarbonitride subfamilies of MXenes. *Nanoscale Horizons* **9**, 1493-1497 (2024).
38. Y. Yang *et al.*, Distinguishing electronic contributions of surface and sub-surface transition metal atoms in Ti-based MXenes. *2D Materials* **7**, (2020).
39. A. D. Handoko *et al.*, Tuning the Basal Plane Functionalization of Two-Dimensional Metal Carbides (MXenes) To Control Hydrogen Evolution Activity. *ACS Applied Energy Materials* **1**, 173-180 (2017).
40. M. Han *et al.*, Beyond $Ti_3C_2T_x$: MXenes for Electromagnetic Interference Shielding. *ACS Nano* **14**, 5008-5016 (2020).
41. K. Jin *et al.*, Tailoring the physical properties of Ni-based single-phase equiatomic alloys by modifying the chemical complexity. *Scientific Reports* **6**, 20159 (2016).
42. S. K. Dewangan, C. Nagarjuna, V. Kumar, in *High Entropy Materials*. (CRC Press), pp. 91-106.
43. M. Han *et al.*, Tailoring Electronic and Optical Properties of MXenes through Forming Solid Solutions. *Journal of the American Chemical Society* **142**, 19110–19118 (2020).
44. M. Khazaei, M. Arai, T. Sasaki, M. Estili, Y. Sakka, Two-dimensional molybdenum carbides: potential thermoelectric materials of the MXene family. *Physical Chemistry Chemical Physics* **16**, 7841-7849 (2014).
45. M. Han *et al.*, Versatility of infrared properties of MXenes. *Materials Today* **64**, 31-39 (2023).
46. Y. Jien-Wei, Recent progress in high entropy alloys. *Ann. Chim. Sci. Mat* **31**, 633-648 (2006).

Acknowledgments: BCW, YY, TP, YM, FU, GK, MT, SKN, AB, HF, KK, BGW, RD, AT, SS, ZF, YG, AV, DJ, and BA would like to acknowledge the National Science Foundation for funding this project under the Center for Chemical Innovation (NSF CCI) program grant 2318105. BCW, SKN, AB, KK, BGW, RD, AT, and BA would also like to thank the National Science Foundation for partially funding this project under the Solid State & Materials Chemistry (NSF SSMC) program grant 2419026. We would also like to thank Professor Thomas E. Mallouk of the University of Pennsylvania for giving us access to the UV-Vis-NIR spectrometer and the Harrick Plasma Cleaner. GK would like to thank Richard Stephens for providing ideas for optimizing the research measurements. SPM and ZDH were supported by Laboratory Directed Research and Development (LDRD) funding from Argonne National Laboratory, provided by the Director, Office of Science, of the U.S. Department of Energy under Contract No. DE-AC02-06CH11357. JJ, NG, and XX acknowledge the support of the National Science Foundation (CBET-2051525). YM would like to thank the Vagelos Institute for Energy Science and Technology (University of Pennsylvania) for support through a graduate fellowship. YM and AV acknowledge the use of the resources of the National Energy Research Scientific Computing Center, a DOE Office of Science User Facility supported by the Office of Science of the U.S. Department of Energy under Contract No. DE-AC02-05CH11231 using NERSC award BES-ERCAP0023161. We also thank the Integrated Nanosystems Development Institute of Indiana University Indianapolis as well as the National Science Foundation Major Research Instrumentation Program for the use of their SEM and XRD equipment (Award 1229514 for SEM and Award 1429241 for XRD).

Author contributions:

Conceptualization: BCW, BA

Methodology: BCW, PM, YG, AV, DJ, BA

Investigation: BCW, YY, PM, TP, YM, FU, GK, MT, SPM, SKN, AB, HF, JJ, KK, BGW, RD, AT, SS, NG

Project Administration: BCW, ZF, YG, AV, DJ, BA

Supervision: ZF, YG, AV, DJ, BA

Writing – original draft: BCW, YY, TP, GK, JJ, KK

Writing – review & editing: All authors

Competing interests:

BCW and BA declare that a provisional patent on the synthesis of high-entropy MAX phases has been filed under patent number 70880-01. All other authors declare no competing interests.

Data availability:

All data, code, and information reported in the main text and supporting information or otherwise used in the preparation of this work will be made upon reasonable requests to the corresponding authors.

Supplementary Materials:

Materials and Methods

Supplementary Text

Figs. S1 to S72

Tables S1 to S2

References (*1-16*)